

On deep squeezing or cooling a parametric resonator using feedback

Adriano A. Batista^{1*} and Raoni S. N. Moreira², and A. A. Lisboa de Souza³

¹ *Departamento de Física, Universidade Federal de Campina Grande*

Campina Grande-PB, CEP: 58429-900, Brazil

² *Departamento de Física, Universidade Federal de Pernambuco, 50670-901 Recife-PE, Brazil*

³ *Departamento de Engenharia Elétrica, Universidade Federal da Paraíba*

João Pessoa-PB, CEP: 58.051-970, Brazil

(Dated: May 1, 2026)

Abstract

Here we analyze ways to achieve deep subthreshold parametric squeezing or cooling of a parametric resonator enhanced by a lock-in amplifier feedback loop. Due to this feedback, the dynamics of the parametric resonator becomes more complex and a Hopf bifurcation at the instability threshold can occur. Initially, to obtain insight on this system, we calculate the phase-dependent gain in the response to an added ac signal. We calculate this amplification gain approximately using two independent techniques: the averaging method and the harmonic balance method. We also obtain this gain more precisely using Floquet theory and Green's functions. The Hopf bifurcation was predicted by the harmonic balance method and by Floquet theory, but not by the averaging method. In our analysis of fluctuations, we Fourier analyze the response of the parametric resonator with feedback to an added white noise. We were able to calculate, in addition to the noise spectral density, the squeezing of fluctuations. Deamplification and cooling occur near the Hopf bifurcation, whereas deep squeezing and heating occurs near a saddle-node bifurcation. Our results show that the averaging method, a widely-used perturbative technique, fails in the analysis of fluctuations near a Hopf bifurcation. Direct application of the averaging method to stochastic differential equations should be compared to other techniques such as Floquet theory (FT) or Fourier analysis whenever possible. The novel cooling technique presented here may have wide applications in increasing the sensitivity of resonant detectors and sensors.

* adriano@df.ufcg.edu.br

I. INTRODUCTION

Parametric modulation offers a powerful route for suppressing fluctuations in resonators across physics and engineering [1], enabling both phase-dependent amplification and squeezing. It has been used to enhance the sensitivity of gravitational-wave detectors [2, 3], for preparing nonclassical states of mechanical resonators [4, 5], for implementing very sensitive accelerometers [6], force [7] and mass sensors [8, 9]. More recently, parametric modulation has played a fundamental role in the phase state qubit implementation in Kerr parametric oscillators [10, 11]. Despite of these advances, conventional parametric schemes face two fundamental limits: squeezing is bounded to -6 dB at the instability threshold [12, 13] and cooling is not possible. Feedback control provides an alternate strategy without these limitations, but its combination with parametric modulation has remained largely unexplored from a theoretical standpoint. In this work, we fill that gap by analyzing a single-degree-of-freedom (SDOF) parametric resonator augmented with a lock-in amplifier feedback loop that can be tuned to either squeeze or cool.

The thermo-mechanical squeezing limitation was overcome only in 2013 by Vinante and Falferi in Ref. [14]. In their work, a -11.3 dB in squeezing of thermal fluctuations of a parametrically modulated microscopic silicon beam cantilever was reached experimentally with the assistance of feedback. Further experimental advances using the same squeezing technique with parametric pump and feedback were subsequently made by Poot *et al.* [15], Sonar *et al.* [16], and Mashaal *et al.* [17]. Although these papers advanced the experimental implementation of thermomechanical squeezing enhanced by feedback, they did not advance the theoretical analysis of fluctuations developed by Vinante and Falferi. Their model oversimplifies the dynamics of the parametric resonator with feedback by averaging the equations of motion from the start, what reduced the dynamical system dimensions. Consequently, this led to their missing of a Hopf bifurcation. In addition to that, they did not provide a way to calculate the NSD of the parametric resonator fluctuations nor the NSD of the lockin outputs.

Another method used to reduce fluctuations is cooling. It can be implemented in optomechanical resonators in several ways: parametric feedback [18–20], feedback [21–24], sideband [25], and radiation pressure [26]. Effective temperatures as low as a few millikelvin can be achieved using these feedback schemes. Even quantum ground state cooling has been implemented experimentally in nanomechanical resonators [27]. The comprehensive review of cavity optomechanics by Aspelmeyer *et al.* [4] has many more citations on cooling resonators. The feedback scheme

analyzed here is capable of achieving cooling and it could be applied and tested in various types of physical systems.

Here we extend our previous works on fluctuations and on squeezing of fluctuations in parametrically-modulated resonators with added noise [28, 29] by including feedback. Specifically, we analyze a linear feedback scheme inspired by the one proposed by Vinante and Falferi to cool or enhance squeezing of fluctuations. When the parametric resonator with feedback is excited by an added ac signal, without noise, we analytically obtain the gain curve as a function of phase using the averaging method (AM) and the harmonic balance method (HBM). We show that the SDOF parametric resonator with feedback has a higher dynamical dimensionality, with three Floquet multipliers, what allows Hopf bifurcations. We find that this is a new route to instability, in addition to period-doubling or saddle-node bifurcations. The analytical results of this approach are verified with numerical results based on FT. This analysis of a deterministic stationary response complements our stochastic analysis of squeezing and cooling. It is a way to independently check our results. Subsequently, in our analysis of fluctuations, we avoid directly averaging the stochastic differential equations. Instead, we use the Green's functions method in the frequency domain. We obtain the Green's functions, approximately, using a perturbative Fourier transform method or, more exactly, using FT. With this method, we calculate the noise spectral density (NSD) of the resonator response to the added noise. We also obtain the dispersions in the sine and cosine quadratures at half the pump frequency and the correlation that arises between these quadratures. Our results go beyond the -6 dB limit, predict a new instability route via Hopf bifurcation, and provide a consistent stochastic theory that has been missing in previous experimental work on feedback-enhanced squeezing.

The remainder of this paper is organized as follows. In Sec. II we initially analyze degenerate parametric amplification of an ac signal enhanced by the proposed lock-in amplifier (LIA) feedback scheme using the AM, the HBM, and FT. We also predict the Hopf bifurcation line analytically. In Sec. III we analyze the corresponding stochastic model in which the ac signal is replaced by white noise. We calculate the NSD and obtain analytical expressions for the enhanced squeezing or cooling of fluctuations. In Sec. IV we analyze and discuss our numerical results, and in Sec. V we draw our conclusions.

II. PARAMETRIC AMPLIFICATION WITH LOCKIN FEEDBACK

Here we analyze degenerate parametric amplification enhanced by LIA feedback in a SDOF parametric amplifier. The objective being to obtain threshold lines to instability and the gain curve as a function of the signal phase. This analysis of a deterministic stationary response will guide our subsequent analysis of stochastic processes such as squeezing and cooling. It is a simple way to verify if deep squeezing and cooling are possible.

The equations of motion of the parametric resonator with this feedback scheme is given by the following by following integro-differential equation

$$\ddot{x} + \gamma\dot{x} + \omega_0^2 x - F_p \sin(2\omega t)x = 2\eta \sin(\omega t)X_L(t) + F_s \cos(\omega_s t + \varphi_0), \quad (1)$$

where γ is the dissipation coefficient, ω_0 is the angular natural frequency of the resonator, F_p is the pump amplitude, 2ω is the pump frequency, η is the feedback constant, F_s is the input signal amplitude, ω_s is the input signal angular frequency, φ_0 is the input signal phase, and

$$X_L(t) = \frac{1}{\tau} \int_{-\infty}^t e^{-(t-t')/\tau} \cos(\omega t')x(t') dt' \quad (2)$$

is the first-order RC filter output from the cosine quadrature of a LIA (see the appendix for more details). The above integro-differential equation can be rewritten as the following non-autonomous ordinary differential equation system

$$\begin{aligned} \ddot{x} + \gamma\dot{x} + \omega_0^2 x - F_p \sin(2\omega t)x &= 2\eta \sin(\omega t)z + F_s \cos(\omega_s t + \varphi_0), \\ \dot{z} &= -\frac{z}{\tau} + \cos(\omega t)\frac{x}{\tau}, \end{aligned} \quad (3)$$

where $z(t) = X_L(t)$.

A. The AM analysis of degenerate parametric amplification

Let us analyze the amplification dependence on phase obtained from Eqs. (3) in a similar way to what was performed by Rugar and Grütter in Ref. [12]. This analysis provides us with insight on the response of this system to added noise. We now transform the fast variables $(x(t), \dot{x}(t))$ from Eq. (3) into the slow variables $(\mathcal{U}(t), \mathcal{V}(t))$ via $x(t) = \mathcal{U}(t) \cos \omega t - \mathcal{V}(t) \sin \omega t$ and $\dot{x}(t) = -\omega [\mathcal{U}(t) \sin \omega t + \mathcal{V}(t) \cos \omega t]$. The variable z already varies slowly, as long as $\omega_0\tau \gg 1$, so it does not need to be transformed. We find the equations of motion for $\mathcal{U}(t)$ and $\mathcal{V}(t)$ to be

$$\begin{pmatrix} \dot{\mathcal{U}} \\ \dot{\mathcal{V}} \end{pmatrix} = -\frac{1}{\omega} \begin{pmatrix} \sin \omega t f(x, y, z, t) \\ \cos \omega t f(x, y, z, t) \end{pmatrix}, \quad (4)$$

where $f(x, y, z, t) = -\Omega x + F_p \sin(2\omega t) x - \gamma y + 2\eta z \sin \omega t + F_s \cos(\omega t + \varphi(t))$, with $\Omega = \omega_0^2 - \omega^2$ and $\varphi(t) = \delta t + \varphi_0$, with $\delta = \omega_s - \omega$. Subsequently, we apply the averaging method to these equations and obtain the following averaged dynamical system

$$\begin{aligned} \dot{u} &= -\frac{1}{2\omega} \left[\left(\frac{F_p}{2} + \gamma\omega \right) u + 2\eta z + \Omega v - F_s \sin \varphi(t) \right], \\ \dot{v} &= \frac{1}{2\omega} \left[\Omega u + \left(\frac{F_p}{2} - \gamma\omega \right) v - F_s \cos \varphi(t) \right], \\ \dot{z} &= -\frac{z}{\tau} + \frac{u}{2\tau}, \end{aligned} \quad (5)$$

where $\mathcal{U}(t) \approx u(t)$ and $\mathcal{V}(t) \approx v(t)$. When $\omega = \omega_s$, we can write the fixed-point solution of Eq. (5) as

$$\begin{pmatrix} u \\ v \end{pmatrix} = \frac{F_s}{\left(\frac{F_p}{2} + \gamma\omega + \eta \right) \left(\frac{F_p}{2} - \gamma\omega \right) - \Omega^2} \begin{pmatrix} \frac{F_p}{2} - \gamma\omega & -\Omega \\ -\Omega & \frac{F_p}{2} + \gamma\omega + \eta \end{pmatrix} \begin{pmatrix} \sin \varphi_0 \\ \cos \varphi_0 \end{pmatrix} \quad (6)$$

Consequently, we can write the gain ($r/|\chi(\omega)F_s|$) in the averaging approximation as

$$G_{avg}(\omega, \varphi_0) = \frac{\sqrt{\Omega^2 + \frac{F_p^2}{4} + \gamma^2\omega^2 + \frac{\eta^2}{2} + \eta \left(\frac{F_p}{2} + \gamma\omega \right) + [F_p\gamma\omega + \frac{\eta}{2}(\eta + F_p + 2\gamma\omega)] \cos 2\varphi_0 - \Omega(F_p + \eta) \sin 2\varphi_0}}{\left| \left(\frac{F_p}{2} + \gamma\omega + \eta \right) \left(\frac{F_p}{2} - \gamma\omega \right) - \Omega^2 \right| |\chi(\omega)|}, \quad (7)$$

where $r^2 = u^2 + v^2$ and $\chi(\omega) = \frac{1}{\omega_0^2 - \omega^2 - i\gamma\omega}$ is the susceptibility. Based on Eq. (7), we obtain that the instability threshold of parametric oscillations with lock-in feedback is given by

$$F_p^2 + 2\eta F_p - 4(\gamma^2\omega^2 + \Omega^2 + \eta\gamma\omega) = 0 \implies F_p = -\eta \pm \sqrt{4\Omega^2 + (\eta + 2\gamma\omega)^2} \quad (8)$$

From Eq. (7), we find the minimum and maximum gain of the response of the parametric amplifier at zero detuning ($\Omega = 0$) to be

$$\begin{aligned} G_{avg}^{min} &= \frac{r_{min}}{r_0} = \frac{\gamma\omega}{|F_p/2 + \gamma\omega + \eta|}, \\ G_{avg}^{max} &= \frac{r_{max}}{r_0} = \frac{\gamma\omega}{|F_p/2 - \gamma\omega|}, \end{aligned} \quad (9)$$

where $r_0 = |\chi(\omega)F_s|$ is the forced harmonic oscillator amplitude.

B. The HBM analysis of degenerate parametric amplification

We seek a stationary solution to the integro-differential equation (1) in the form

$$x(t) = \frac{1}{2} [A_x(\omega)e^{-i\omega t} + A_x^*(\omega)e^{i\omega t}]. \quad (10)$$

With this substitution in Eq. (2) we obtain

$$X_L(t) = \frac{1}{4} \left[A_x + A_x^* + \frac{A_x e^{-2i\omega t}}{1 - 2i\omega\tau} + \frac{A_x^* e^{2i\omega t}}{1 + 2i\omega\tau} \right].$$

Using the fact that the functions $e^{\pm i\omega t}$ are linearly independent, we find

$$\begin{aligned} \left[1 - \eta \frac{\chi(\omega)\omega\tau}{1 - 2i\omega\tau} \right] A_x - i \frac{\chi(\omega)}{2} (F_p + \eta) A_x^* &= \chi(\omega) F_s e^{-i\varphi_0}, \\ \left[1 - \eta \frac{\chi^*(\omega)\omega\tau}{1 + 2i\omega\tau} \right] A_x^* + i \frac{\chi^*(\omega)}{2} (F_p + \eta) A_x &= \chi^*(\omega) F_s e^{i\varphi_0}, \end{aligned} \quad (11)$$

which in matrix format can be written as

$$\begin{pmatrix} 1 - \eta \frac{\chi(\omega)\omega\tau}{1 - 2i\omega\tau} & -i \frac{\chi(\omega)}{2} (F_p + \eta) \\ i \frac{\chi^*(\omega)}{2} (F_p + \eta) & 1 - \eta \frac{\chi^*(\omega)\omega\tau}{1 + 2i\omega\tau} \end{pmatrix} \begin{pmatrix} A_x \\ A_x^* \end{pmatrix} = F_s \begin{pmatrix} \chi(\omega) e^{-i\varphi_0} \\ \chi^*(\omega) e^{i\varphi_0} \end{pmatrix}. \quad (12)$$

The solution is given by

$$\begin{pmatrix} A_x \\ A_x^* \end{pmatrix} = \frac{F_s}{\det M} \begin{pmatrix} 1 - \eta \frac{\chi^*(\omega)\omega\tau}{1 + 2i\omega\tau} & i \frac{\chi(\omega)}{2} (F_p + \eta) \\ -i \frac{\chi^*(\omega)}{2} (F_p + \eta) & 1 - \eta \frac{\chi(\omega)\omega\tau}{1 - 2i\omega\tau} \end{pmatrix} \begin{pmatrix} \chi(\omega) e^{-i\varphi_0} \\ \chi^*(\omega) e^{i\varphi_0} \end{pmatrix}, \quad (13)$$

where

$$\det M = \left| 1 - \frac{\eta\chi(\omega)\omega\tau}{1 - 2i\omega\tau} \right|^2 - \frac{|\chi(\omega)|^2}{4} (F_p + \eta)^2. \quad (14)$$

The transition to parametric instability occurs when $\det M = 0$. In the limit $\omega\tau \rightarrow \infty$, we obtain the same expression for the threshold in the first-order AM approximation given in Eq. (8). The expression for gain with respect to the forced harmonic oscillator response in the HBM approximation can be written as

$$G_{HBM}(\omega, \varphi_0) = \frac{|A_x(\omega, \varphi_0)|}{|\chi(\omega) F_s|}. \quad (15)$$

From this, we find that the minimum and maximum gains are given by

$$\begin{aligned} G_{HBM}^{min}(\omega) &= \frac{1}{\left| 1 - \frac{\eta\chi(\omega)\omega\tau}{1 - 2i\omega\tau} \right| + \frac{|\chi(\omega)|}{2} |F_p + \eta|}, \\ G_{HBM}^{max}(\omega) &= \frac{1}{\left| \left| 1 - \frac{\eta\chi(\omega)\omega\tau}{1 - 2i\omega\tau} \right| - \frac{|\chi(\omega)|}{2} |F_p + \eta| \right|}. \end{aligned} \quad (16)$$

C. Floquet theory analysis of degenerate parametric amplification

According to Ref. [28], the response in frequency space of the parametrically driven resonator to an added signal is given by

$$\tilde{X}(\nu) \approx \tilde{\mathbf{G}}_0(\nu) \tilde{F}(\nu) + \mathbf{G}_+(\nu) \tilde{F}(\nu - 2\omega) + \mathbf{G}_+^*(-\nu) \tilde{F}(\nu + 2\omega). \quad (17)$$

The i -th component response is given by

$$\tilde{X}_i(\nu) \approx \sum_j \tilde{G}_{0,ij}(\nu) \tilde{F}_j(\nu) + \sum_j G_{+,ij}(\nu) \tilde{F}_j(\nu - 2\omega) + \sum_j G_{+,ij}^*(-\nu) \tilde{F}_j(\nu + 2\omega), \quad (18)$$

In the present case of Eq. (3), we have

$$X(t) = \begin{pmatrix} X_0(t) \\ X_1(t) \\ X_2(t) \end{pmatrix} = \begin{pmatrix} x \\ \dot{x} \\ z \end{pmatrix} \quad (19)$$

and

$$F(t) = \begin{pmatrix} 0 \\ \cos(\omega_s t + \varphi_0) \\ 0 \end{pmatrix} \implies \tilde{F}(\nu) = \pi \begin{pmatrix} 0 \\ e^{i\varphi_0} \delta(\nu + \omega_s) + e^{-i\varphi_0} \delta(\nu - \omega_s) \\ 0 \end{pmatrix} \quad (20)$$

The response of the parametric amplifier is given by

$$\begin{aligned} \tilde{x}(\nu) &= \tilde{G}_{0,01}(\nu) \tilde{F}_1(\nu) + G_{+,01}(\nu) \tilde{F}_1(\nu - 2\omega) + G_{+,01}^*(-\nu) \tilde{F}_1(\nu + 2\omega) \\ &= \pi \left[\tilde{G}_{0,01}(\omega_s) e^{-i\varphi_0} \delta(\nu - \omega_s) + \tilde{G}_{0,01}(-\omega_s) e^{i\varphi_0} \delta(\nu + \omega_s) \right] \\ &\quad + \pi \left[G_{+,01}(2\omega + \omega_s) e^{-i\varphi_0} \delta(\nu - 2\omega - \omega_s) + G_{+,01}(2\omega - \omega_s) e^{i\varphi_0} \delta(\nu - 2\omega + \omega_s) \right] \\ &\quad + \pi \left[G_{+,01}^*(2\omega + \omega_s) e^{i\varphi_0} \delta(\nu + 2\omega + \omega_s) + G_{+,01}^*(2\omega - \omega_s) e^{-i\varphi_0} \delta(\nu + 2\omega - \omega_s) \right]. \end{aligned} \quad (21)$$

We then Fourier transform the above equation back to the time domain and find

$$\begin{aligned} x(t) &= \frac{1}{2} \left[\tilde{G}_{0,01}(\omega_s) e^{-i\varphi_0} e^{-i\omega_s t} + \tilde{G}_{0,01}(-\omega_s) e^{i\varphi_0} e^{i\omega_s t} \right] \\ &\quad + \frac{1}{2} \left[G_{+,01}(2\omega + \omega_s) e^{-i\varphi_0} e^{-i(2\omega + \omega_s)t} + G_{+,01}(2\omega - \omega_s) e^{i\varphi_0} e^{-i(2\omega - \omega_s)t} \right] \\ &\quad + \frac{1}{2} \left[G_{+,01}^*(2\omega + \omega_s) e^{i\varphi_0} e^{i(2\omega + \omega_s)t} + G_{+,01}^*(2\omega - \omega_s) e^{-i\varphi_0} e^{i(2\omega - \omega_s)t} \right] \\ &\approx \frac{1}{2} \left[\tilde{G}_{0,01}(\omega_s) e^{-i\varphi_0} e^{-i\omega_s t} + \tilde{G}_{0,01}(-\omega_s) e^{i\varphi_0} e^{i\omega_s t} \right] + \frac{1}{2} \left[G_{+,01}(\omega_i) e^{i\varphi_0} e^{-i\omega_i t} + G_{+,01}^*(\omega_i) e^{-i\varphi_0} e^{i\omega_i t} \right] \\ &= \frac{1}{2} \left[\tilde{G}_{0,01}(\omega_s) e^{-i\varphi_0} e^{-i\delta t} + G_{+,01}(\omega_i) e^{i\varphi_0} e^{i\delta t} \right] e^{-i\omega t} + \frac{1}{2} \left[\tilde{G}_{0,01}^*(\omega_s) e^{i\varphi_0} e^{i\delta t} + G_{+,01}^*(\omega_i) e^{-i\varphi_0} e^{-i\delta t} \right] e^{i\omega t} \end{aligned} \quad (22)$$

where we used $\omega_s = \omega + \delta$ and $\omega_i = \omega - \delta$. Hence, we find that the positive and negative envelopes of $x(t)$ are given by

$$\pm \left| \tilde{G}_{0,01}(\omega_s) e^{-i\varphi_0} e^{-i\delta t} + G_{+,01}(\omega_i) e^{i\varphi_0} e^{i\delta t} \right|. \quad (23)$$

At $\delta = 0$, we obtain the FT expression for the gain

$$G_{FT}(\varphi_0) = \left| \tilde{G}_{0,01}(\omega) + G_{+,01}(\omega) e^{2i\varphi_0} \right|. \quad (24)$$

D. The HBM approximation to the Hopf bifurcation line

We seek a quasi-periodic solution to Eqs. (3) at a Hopf bifurcation point in the following form

$$\begin{aligned} x(t) &= \frac{1}{2} [Ae^{-i(\omega-\Delta)t} + A^*e^{i(\omega-\Delta)t}] + \frac{1}{2} [Be^{-i(\omega+\Delta)t} + B^*e^{i(\omega+\Delta)t}], \\ z(t) &= \frac{1}{2} [Ce^{-i\Delta t} + C^*e^{i\Delta t}]. \end{aligned} \quad (25)$$

We find the algebraic equations

$$\begin{aligned} [\omega_0^2 - (\omega - \Delta)^2 - i\gamma(\omega - \Delta)] A - i\frac{F_p}{2}B^* &= i\eta C^*, \\ [\omega_0^2 - (\omega + \Delta)^2 - i\gamma(\omega + \Delta)] B - i\frac{F_p}{2}A^* &= i\eta C, \\ -i\Delta C &= -\frac{C}{\tau} + \frac{A^* + B}{2\tau} \implies C = \frac{A^* + B}{2(1 - i\tau\Delta)}. \end{aligned} \quad (26)$$

By replacing C in the above expressions, we obtain

$$\begin{aligned} \left[1 - \frac{i\eta\chi(\omega - \Delta)}{2(1 + i\tau\Delta)}\right] A - i\frac{\chi(\omega - \Delta)}{2} \left[F_p + \frac{\eta}{1 + i\tau\Delta}\right] B^* &= 0, \\ i\frac{\chi^*(\omega + \Delta)}{2} \left[F_p + \frac{\eta}{(1 + i\tau\Delta)}\right] A + \left[1 + \frac{i\eta\chi^*(\omega + \Delta)}{2(1 + i\tau\Delta)}\right] B^* &= 0. \end{aligned} \quad (27)$$

We find the characteristic equation (a necessary condition for nontrivial solutions) to be

$$\left[1 - \frac{i\eta\chi(\omega - \Delta)}{2(1 + i\tau\Delta)}\right] \left[1 + \frac{i\eta\chi^*(\omega + \Delta)}{2(1 + i\tau\Delta)}\right] - \frac{\chi(\omega - \Delta)\chi^*(\omega + \Delta)}{4} \left[F_p + \frac{\eta}{1 + i\tau\Delta}\right]^2 = 0. \quad (28)$$

This can be simplified to

$$F_p^2(1 + i\tau\Delta) + 2F_p\eta = 4\eta\omega(\gamma + 2i\Delta) + \frac{4(1 + i\tau\Delta)}{\chi(\omega - \Delta)\chi^*(\omega + \Delta)} \quad (29)$$

Taking the real and imaginary parts of the characteristic equation, we find

$$\begin{aligned} F_p^2 + 2\eta F_p &= 4\eta\omega\gamma + \operatorname{Re} \left\{ \frac{4}{\chi(\omega - \Delta)\chi^*(\omega + \Delta)} \right\} - \operatorname{Im} \left\{ \frac{4\tau\Delta}{\chi(\omega - \Delta)\chi^*(\omega + \Delta)} \right\}, \\ F_p^2 &= \frac{8\eta\omega}{\tau} + \operatorname{Im} \left\{ \frac{4}{\tau\Delta\chi(\omega - \Delta)\chi^*(\omega + \Delta)} \right\} + \operatorname{Re} \left\{ \frac{4}{\chi(\omega - \Delta)\chi^*(\omega + \Delta)} \right\}. \end{aligned} \quad (30)$$

We treat F_p and the detuning Δ as variables to be found after solving the above algebraic system.

III. ANALYSIS OF FLUCTUATIONS

Here we present our theoretical model of fluctuations squeezing by applying LIA feedback to SDOF parametrically-modulated resonators with additive white noise. Specifically, we analyze and generalize the linear feedback scheme proposed by Vinante and Falferi [14] to enhance

squeezing of fluctuations beyond the -6 dB maximum limit previously set by Rugar and Grütter. Afterwards, we analyze the fluctuations in the frequency domain by Fourier transforming the time-dependent stochastic differential (or Langevin) equations of our model into an algebraic stochastic system in the frequency domain. With this procedure we obtain perturbative approximations to the Green's functions in the frequency domain. After this point, we apply the same steps developed in Ref. [29] to obtain the NSD in addition to the dispersions in the sine and cosine quadratures plus their correlation at half the pump frequency. Finally, we apply FT to obtain more exact Green's functions of this model and repeat the calculations to obtain the NSD and the squeezing.

A. Fourier transform approach

The Langevin equation of a damped parametrically driven oscillator with added noise and with feedback from the cosine output of a LIA is given by

$$\begin{aligned}\ddot{x} + \gamma\dot{x} + \omega_0^2 x - F_p \sin(2\omega t)x &= \frac{2\eta}{\tau} \sin(\omega t)z + r(t), \\ \dot{z} &= -\frac{z}{\tau} + \cos(\omega t)\frac{x}{\tau},\end{aligned}\tag{31}$$

where $r(t)$ is a zero-mean Gaussian white noise with autocorrelation $\langle r(t)r(t') \rangle = 2D\delta(t-t')$, where D is the noise level. Here we assumed that the LIA has only one-stage low-pass RC filter before its cosine channel output. After Fourier transforming these equations, we find

$$\begin{aligned}\tilde{x}(\nu) + \frac{iF_p\chi(\nu)}{2} [\tilde{x}(\nu + 2\omega) - \tilde{x}(\nu - 2\omega)] &= -\frac{i\eta\chi(\nu)}{\tau} [\tilde{z}(\nu + \omega) - \tilde{z}(\nu - \omega)] + \chi(\nu)\tilde{r}(\nu) \\ \tilde{z}(\nu) &= \frac{\tilde{x}(\nu + \omega) + \tilde{x}(\nu - \omega)}{2(1 - i\nu\tau)}.\end{aligned}\tag{32}$$

By shifting ν in $\tilde{z}(\nu)$ by $\pm\omega$ we find

$$\begin{aligned}\tilde{z}(\nu - \omega) &= \frac{\tilde{x}(\nu) + \tilde{x}(\nu - 2\omega)}{2(1 - i(\nu - \omega)\tau)}, \\ \tilde{z}(\nu + \omega) &= \frac{\tilde{x}(\nu) + \tilde{x}(\nu + 2\omega)}{2(1 - i(\nu + \omega)\tau)}.\end{aligned}$$

Hence, we can now rewrite Eq. (32) in the following format

$$\alpha(\nu)\tilde{x}(\nu) + \beta^*(-\nu)\tilde{x}(\nu - 2\omega) + \beta(\nu)\tilde{x}(\nu + 2\omega) = \chi(\nu)\tilde{r}(\nu),\tag{33}$$

where

$$\begin{aligned}\alpha(\nu) &= 1 + \frac{i\eta\chi(\nu)}{2} \left[\frac{1}{1 - i(\nu + \omega)\tau} - \frac{1}{1 - i(\nu - \omega)\tau} \right], \\ \beta(\nu) &= \frac{i\chi(\nu)}{2} \left[F_p + \frac{\eta}{1 - i(\nu + \omega)\tau} \right].\end{aligned}\tag{34}$$

Using the same type of steps we developed in Ref. [30], we can approximate the solution to Eq. (33) by

$$\tilde{x}(\nu) = \tilde{\mathcal{G}}_0(\nu)\tilde{r}(\nu) + \mathcal{G}_+(\nu)\tilde{r}(\nu - 2\omega) + \mathcal{G}_-(\nu)\tilde{r}(\nu + 2\omega), \quad (35)$$

where

$$\begin{aligned} \tilde{\mathcal{G}}_0(\nu) &= \frac{\chi(\nu)}{\alpha(\nu) - \frac{\beta^*(-\nu)\beta(\nu - 2\omega)}{\alpha(\nu - 2\omega)} - \frac{\beta(\nu)\beta^*(-\nu - 2\omega)}{\alpha(\nu + 2\omega)}}, \\ \mathcal{G}_+(\nu) &= -\frac{\beta^*(-\nu)\chi(\nu - 2\omega)}{\alpha(\nu - 2\omega) \left[\alpha(\nu) - \frac{\beta^*(-\nu)\beta(\nu - 2\omega)}{\alpha(\nu - 2\omega)} - \frac{\beta(\nu)\beta^*(-\nu - 2\omega)}{\alpha(\nu + 2\omega)} \right]}, \\ \mathcal{G}_-(\nu) &= -\frac{\beta(\nu)\chi(\nu + 2\omega)}{\alpha(\nu + 2\omega) \left[\alpha(\nu) - \frac{\beta^*(-\nu)\beta(\nu - 2\omega)}{\alpha(\nu - 2\omega)} - \frac{\beta(\nu)\beta^*(-\nu - 2\omega)}{\alpha(\nu + 2\omega)} \right]}. \end{aligned} \quad (36)$$

Note that $\tilde{\mathcal{G}}_0(-\nu) = \tilde{\mathcal{G}}_0^*(\nu)$, $\mathcal{G}_+(\nu) = \mathcal{G}_*(-\nu)$, and that $\tilde{x}(-\nu) = \tilde{x}^*(\nu)$ as expected since $x(t)$ is a real-valued function.

1. The NSD calculation

In the same way we performed previously in Ref. [31], we can write the NSD of $\tilde{x}(\nu)$, $\tilde{X}_L(\nu)$, and $\tilde{Y}_L(\nu)$, respectively, as

$$\begin{aligned} S_N(\nu) &= 2D \left[|\tilde{\mathcal{G}}_0(\nu)|^2 + |\mathcal{G}_+(\nu)|^2 + |\mathcal{G}_-(\nu)|^2 \right], \\ S_{\tilde{X}_L}(\nu) &= \frac{D}{2} \frac{\left| \tilde{\mathcal{G}}_0(\nu - \omega) + \mathcal{G}_+(\nu + \omega) \right|^2 + \left| \tilde{\mathcal{G}}_0(\nu + \omega) + \mathcal{G}_-(\nu - \omega) \right|^2}{1 + \tau^2\nu^2}, \\ S_{\tilde{Y}_L}(\nu) &= \frac{D}{2} \frac{\left| \tilde{\mathcal{G}}_0(\nu - \omega) - \mathcal{G}_+(\nu + \omega) \right|^2 + \left| \tilde{\mathcal{G}}_0(\nu + \omega) - \mathcal{G}_-(\nu - \omega) \right|^2}{1 + \tau^2\nu^2}. \end{aligned} \quad (37)$$

The functions $S_{\tilde{X}_L}(\nu)$ and $S_{\tilde{Y}_L}(\nu)$ represent the stationary NSDs of the lockin amplifier X and Y channel outputs in the frequency domain. At $\nu = 0$, these results are in agreement with the NSDs for $\tilde{x}'(\omega)$ and $\tilde{x}''(\omega)$. See the appendix and the following discussion on squeezing.

2. The squeezing calculation

We find the same type of expressions for fluctuations squeezing as in Eqs. (29)-(30) of Ref. [29]. We obtain the two dispersions of the real and imaginary parts of $\tilde{x}(\omega)$ and the correlation between

them to be given by

$$\begin{aligned}
\sigma_c^2(\omega) &= \lim_{\Delta\nu \rightarrow 0^+} \int_{\omega-\Delta\nu}^{\omega+\Delta\nu} \langle \tilde{x}'(\omega) \tilde{x}'(\nu') \rangle d\nu' \\
&\approx 2\pi D \left[|\tilde{\mathcal{G}}_0(\omega)|^2 + |\mathcal{G}_+(\omega)|^2 + 2 \operatorname{Re} \left\{ \tilde{\mathcal{G}}_0(\omega) \mathcal{G}_+(\omega) \right\} \right], \\
\sigma_s^2(\omega) &= \lim_{\Delta\nu \rightarrow 0^+} \int_{\omega-\Delta\nu}^{\omega+\Delta\nu} \langle \tilde{x}''(\omega) \tilde{x}''(\nu') \rangle d\nu' \\
&\approx 2\pi D \left[|\tilde{\mathcal{G}}_0(\omega)|^2 + |\mathcal{G}_+(\omega)|^2 - 2 \operatorname{Re} \left\{ \tilde{\mathcal{G}}_0(\omega) \mathcal{G}_+(\omega) \right\} \right], \\
\sigma_{cs}(\omega) &= \lim_{\Delta\nu \rightarrow 0^+} \int_{\omega-\Delta\nu}^{\omega+\Delta\nu} \langle \tilde{x}'(\omega) \tilde{x}''(\nu') \rangle d\nu' = 4\pi D \operatorname{Im} \left\{ \tilde{\mathcal{G}}_0(\omega) \mathcal{G}_+(\omega) \right\}.
\end{aligned} \tag{38}$$

At $\nu = \omega$, we have approximately

$$\begin{aligned}
\tilde{\mathcal{G}}_0(\omega) &\approx \frac{\alpha^*(\omega)\chi(\omega)}{|\alpha(\omega)|^2 - |\beta(-\omega)|^2}, \\
\mathcal{G}_+(\omega) &\approx -\frac{\beta^*(-\omega)\chi^*(\omega)}{|\alpha(\omega)|^2 - |\beta(-\omega)|^2}, \\
\operatorname{Re} \left\{ \tilde{\mathcal{G}}_0(\omega) \mathcal{G}_+(\omega) \right\} &\approx -\frac{\operatorname{Re} \left\{ \alpha^*(\omega) \beta^*(-\omega) \right\}}{(|\alpha(\omega)|^2 - |\beta(-\omega)|^2)^2} |\chi(\omega)|^2, \\
\operatorname{Im} \left\{ \tilde{\mathcal{G}}_0(\omega) \mathcal{G}_+(\omega) \right\} &\approx -\frac{\operatorname{Im} \left\{ \alpha^*(\omega) \beta^*(-\omega) \right\}}{(|\alpha(\omega)|^2 - |\beta(-\omega)|^2)^2} |\chi(\omega)|^2.
\end{aligned} \tag{39}$$

After replacing these expressions in Eq. (38), we obtain the dispersions and correlation to be given by

$$\begin{aligned}
\sigma_c^2(\omega) &\approx 2\pi D \frac{|\alpha^*(\omega) + \beta(-\omega)|^2}{[|\alpha(\omega)|^2 - |\beta(-\omega)|^2]^2} |\chi(\omega)|^2, \\
\sigma_s^2(\omega) &\approx 2\pi D \frac{|\alpha^*(\omega) - \beta(-\omega)|^2}{[|\alpha(\omega)|^2 - |\beta(-\omega)|^2]^2} |\chi(\omega)|^2, \\
\sigma_{cs}(\omega) &\approx -4\pi D \frac{\operatorname{Im} \left\{ \alpha^*(\omega) \beta^*(-\omega) \right\}}{(|\alpha(\omega)|^2 - |\beta(-\omega)|^2)^2} |\chi(\omega)|^2,
\end{aligned} \tag{40}$$

where

$$\begin{aligned}
\alpha(\omega) &= 1 - \frac{\eta\omega\tau\chi(\omega)}{1 - 2i\omega\tau}, \\
\beta^*(-\omega) &= -\frac{i\chi(\omega)}{2}(F_p + \eta).
\end{aligned}$$

Note that if $F_p = \eta = 0$, $\sigma_c^2 = \sigma_s^2 = \sigma_0^2 = 2\pi D |\chi(\omega)|^2$ and $\sigma_{cs} = 0$.

B. Floquet theory approach

We now apply the same FT method developed previously in Refs. [28, 29] to obtain the average fluctuations (the NSDs and the squeezing) of the parametric resonator with LIA feedback. This

became possible because we transformed the original integro-differential model of Eq. (1) into the ODE system with additive noise of Eq. (31). The FT method has one important advantage over the approximate Fourier transform method we developed in the previous section: we can find far more precise estimates for the NSD and for the squeezing.

1. The NSD calculation

We find that the NSD for the SDOF parametric resonator with LIA feedback and additive noise is given by

$$S_N(\nu) = \lim_{\Delta\nu \rightarrow 0^+} \int_{\nu-\Delta\nu}^{\nu+\Delta\nu} \frac{\langle \tilde{x}(-\nu) \tilde{x}(\nu') \rangle}{2\pi} d\nu' = 2D \left(\left| \tilde{G}_{0,01}(\nu) \right|^2 + |G_{+,01}(\nu)|^2 + |G_{-,01}(\nu)|^2 \right), \quad (41)$$

where the additive noise vector is given by

$$R(t) = \begin{pmatrix} 0 \\ r(t) \\ 0 \end{pmatrix}. \quad (42)$$

The Green's functions in the frequency domain are obtained from applying FT to Eq. (31) and using the techniques developed in Ref. [28].

2. The squeezing calculation

The calculation of the cosine and sine quadrature dispersions is performed in the same way as in Eqs. (38), but with $\tilde{\mathcal{G}}_0(\omega)$ and $\mathcal{G}_+(\pm\omega)$ replaced by $\tilde{G}_{0,01}(\omega)$ and $G_{+,01}(\pm\omega)$, respectively.

IV. NUMERICAL RESULTS AND DISCUSSION

In Fig. 1 we show the instability threshold lines of the parametric resonator with LIA feedback as described by Eq. (3). In panel **A** the threshold lines are obtained approximately via the averaging or the HBM, or more exactly via the FT method. The dotted blue line is obtained from the averaging approximation, Eq. (8), while the dashed line is obtained by HBM, Eq. (14). The threshold obtained by FT occurs when one or two of the multipliers reach module 1. One can see an excellent agreement between the HBM predictions with FT results for the instability line. The averaging approximation is also good, but it is slightly off for increasing detuning. In panel **B** the

averaging approximation to instability breaks down and also the usual HBM approximation. A Hopf bifurcation occurs and one has to assume a quasi-periodic solution as given in Eq. (25) at the threshold. The dashed threshold line is obtained from the solution of Eq. (30). This line agrees with the FT prediction for instability.

In Fig. 2 **A** we plot the Floquet multipliers in the complex plane as the pump amplitude F_p is varied from 0 to 0.002. A saddle-node bifurcation occurs at $F_p \approx 0.002$ when the real FM reaches the value 1 while the complex FMs still have magnitude less than 1. In panel **B** we plot the Floquet multipliers in the complex plane as F_p is varied from 0 to -0.042 (there is a phase of 180° in the pump relative to the pump in panel **A**). For $F_p = -0.042$, the complex conjugate pair of multipliers reaches module 1 while the real multiplier has module less than 1. This is a hallmark of a Hopf bifurcation. This bifurcation is only possible because the dynamical system of Eq. (3) has three Floquet multipliers and also because the product of these multiplies, according to Liouville's formula, is $\mu_1\mu_2\mu_3 = e^{-2\pi(\gamma+\tau^{-1})/\omega} < 1$ for any set of parameters.

In Fig. 3 **A** we show a transient of $x(t)$ obtained from numerical integration. The parameters are set near a Hopf bifurcation. One clearly sees that the averaging method does not account for the Hopf bifurcation as cyclo-stationary oscillations emerge as the fast decaying transient dies out. In panel **B** we plot the Fourier transform of the stationary part of the time series shown in panel **A**. The two peaks are a signature of the quasi-periodic behavior that arises near the onset of a Hopf bifurcation. The dashed lines were obtained from the harmonic balance method by solving Eq. (30).

In Fig. 4 **A**, we show a normalized cyclo-stationary response to the ac excitation at angular frequency ω_s which is slightly detuned from half the pump frequency ω . The envelopes obtained from FT provide an excellent fit for the oscillations. The parameters are set near the onset of a saddle-node bifurcation. In panel **B**, we achieve very deep deamplification around -60 dB, which is much less than the -6 dB lower limit of standard parametric deamplification. This shows that deep squeezing can be obtained in the SDOF parametric resonator with LIA feedback.

In Fig. 5 **A**, we again show a normalized cyclo-stationary response to the ac excitation at angular frequency ω_s which is slightly detuned from half the pump frequency ω . The response of the SDOF parametric resonator with feedback is far reduced compared with the amplitude of the harmonic oscillator response. The parameters are set near the onset of a Hopf bifurcation. In panel **B** we plot the gain as a function of phase for the SDOF parametric amplifier with LIA feedback as described in Eq. (3). There is attenuation in all phases. This indicates that with the chosen parameters the

parametric resonator with feedback experiments cooling.

In Fig. 6, we show various scaled NSDs: the harmonic oscillator (the blue solid line), parametric resonator without feedback (the solid green line with \times symbol) was obtained from the HBM, whereas the yellow dot-dashed line was obtained from FT). The SDOF parametric resonator with LIA feedback: positive pump (the solid red line, using the HBM, and dotted black line, using FT), negative pump (solid green line (HBM) and dashed black line (FT)). The FT and HBM yield basically the same results for the NSDs (at least in the dB scale). We find the effective temperature of the resonator with the parameters $F_p = -0.02$ and $\eta = 1$ is roughly 5×10^{-3} of the temperature T of the harmonic oscillator in thermal equilibrium. The two sideband peaks in some of the NSDs are due to the complex conjugate pair of Floquet exponents [28]. If the pump becomes more negative the sideband peaks grow and the resonator warms again as one nears the Hopf instability line.

In Fig. 7, we plot the temperature as a function of F_p . The minimum value of the largest FM in amplitude, $|\mu_{max}|$, is given by $e^{-2\pi(\gamma+\tau^{-1})/(3\omega)}$ from Liouville's formula. While this does not correspond to the minimum value of the effective temperature, it provides an approximate estimate for pump value. Based on the above expression, $\tau > 0$ should be as small as possible for smaller effective temperatures, but it cannot be zero, otherwise, the dynamical system dimensions reduces to 2. There should be an optimum τ . If the parametric resonator is in a heat bath, then $\gamma \propto D$, hence by increasing γ the noise level also increases, hence increasing γ is not a good strategy for lowering the effective temperature. The minimum temperature reached should correspond to the most efficient cooling.

In Fig. 8, we can see that very deep squeezing is achieved for various values of ω . One sees very little dependence of the smallest dispersion on F_p , whereas the larger dispersion grows continuously from the smallest value near the Hopf bifurcation until it diverges at the saddle-node bifurcation. When $\omega = \omega_0$, the squeezing is strongest and there is also cooling near the Hopf bifurcation. These phenomena become weaker as detuning increases. The derivation of the diagonalization of the standard deviations in the squeezing phenomenon is described in the appendix of Ref. [29]. We obtained these results independently using the HBM and FT. One can see a perfect agreement between them.

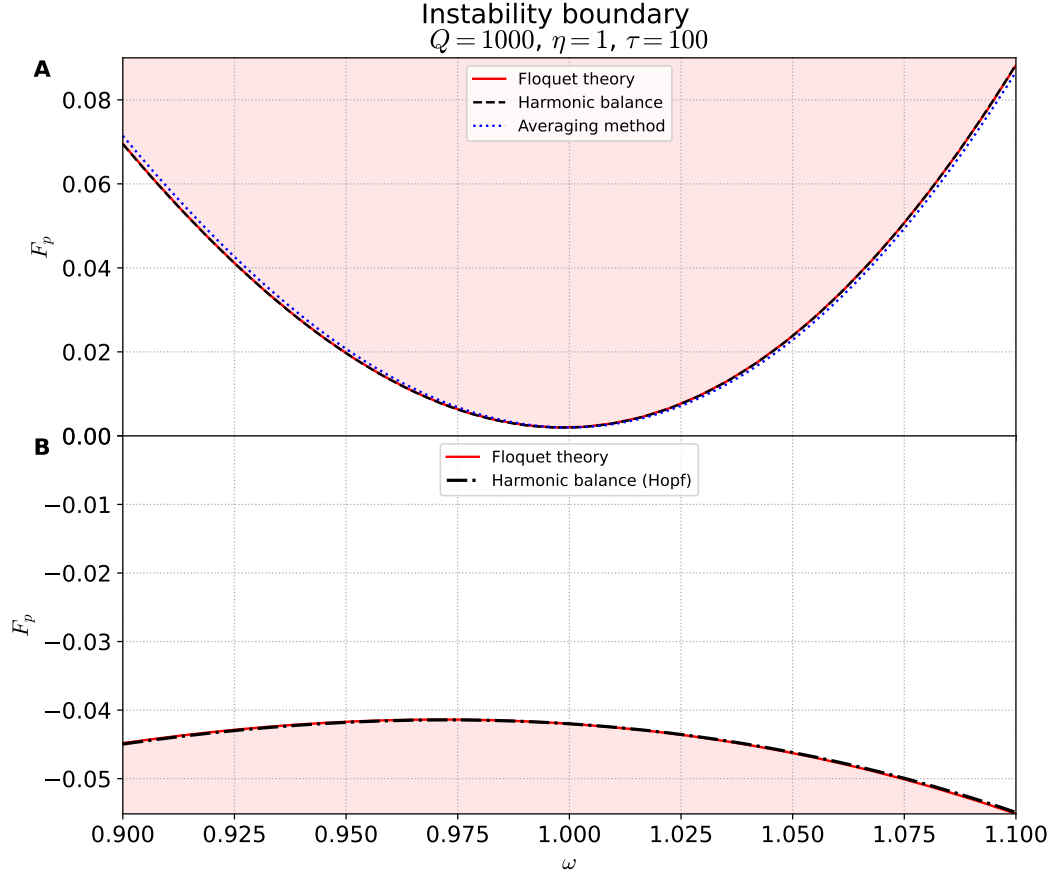


FIG. 1. Parametric instability threshold line for the SDOF parametric resonator with LIA feedback as described by Eq. (3) with $F_s = 0$. **A** The threshold line to instability occurs at a saddle-node bifurcation (when one real Floquet multiplier becomes equal to 1). Comparison between the FT prediction, the HBM prediction (from the characteristic equation $\det M = 0$ in Eq. (14)), and the averaging prediction (the positive root of Eq. (8)). **B** The threshold line to instability occurs at a Hopf bifurcation (when the module of the complex conjugate pair of Floquet multipliers becomes equal to 1). Comparison between FT prediction and the HBM prediction, which is obtained from solving the algebraic system from Eq. (30).

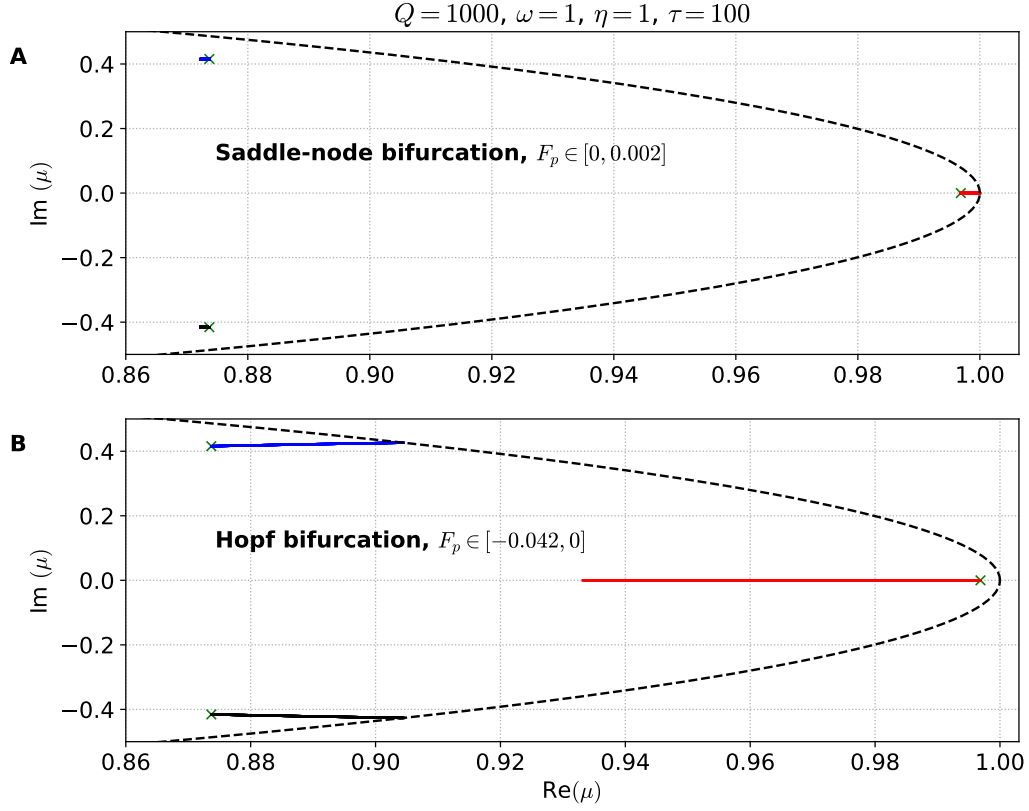


FIG. 2. Plots of the Floquet multipliers as the pump amplitude is varied for the parameters shown at the top of the figure. The vertical axis was compressed for better visibility. The dashed line corresponds to the instability threshold at $|\mu| = 1$. The 'x' symbols represent the Floquet multipliers at $F_p = 0$. **A** The pump amplitude F_p is varied from 0 to 0.002. A saddle-node bifurcation occurs at $F_p \approx 0.002$ when the real FM reaches the values 1 while the complex FMs still have magnitude less than 1. **B** The pump amplitude F_p is varied from 0 to -0.042 . A Hopf bifurcation occurs at $F_p \approx -0.042$ when the pair of complex FMs reaches the unit circle while the real FM still has magnitude less than 1.

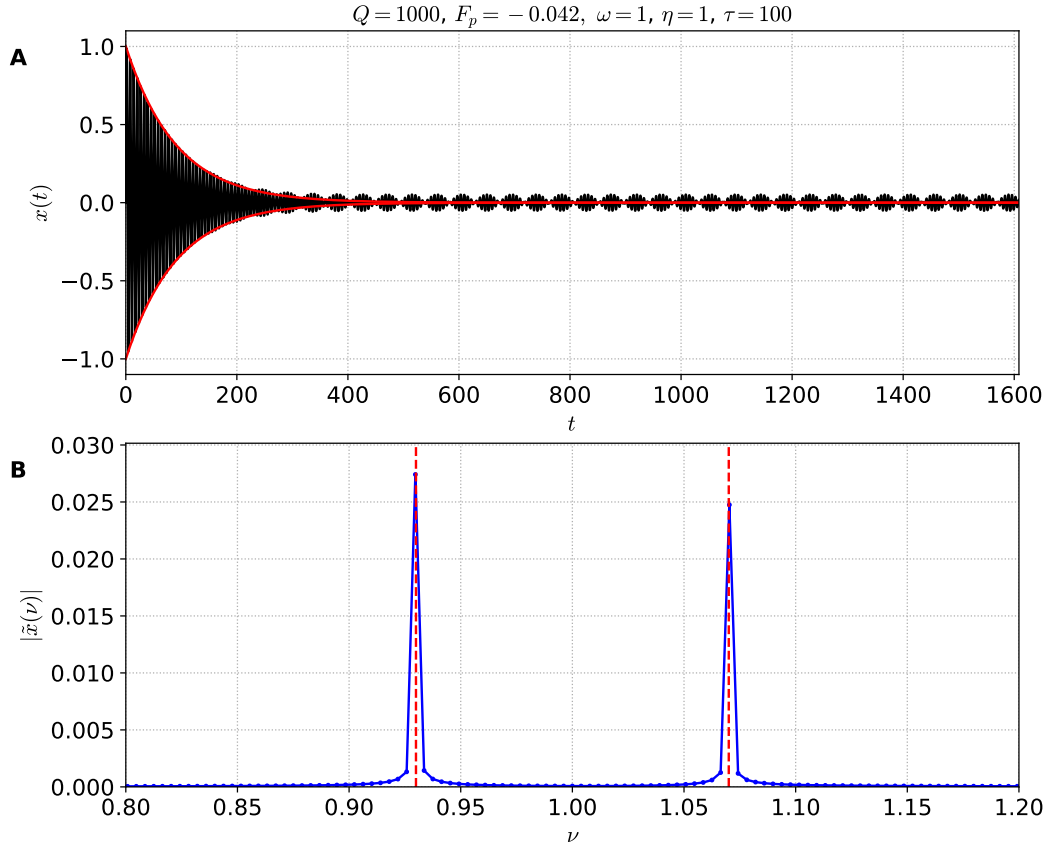


FIG. 3. **A** A time-series transient of $x(t)$ obtained from numerical integration of Eqs. (3) with parameters set near a Hopf bifurcation point. The envelopes (red lines) are obtained from the averaging approximation by integrating Eqs. (5). The envelopes are given by $\pm\sqrt{u^2(t) + v^2(t)}$. **B** Fourier transform of the stationary part of the time series shown in panel **A**. The two peaks are a signature of quasi-periodic behavior that arises near the onset of a Hopf bifurcation. The dashed lines were obtained from the harmonic balance method by solving Eq. (30).

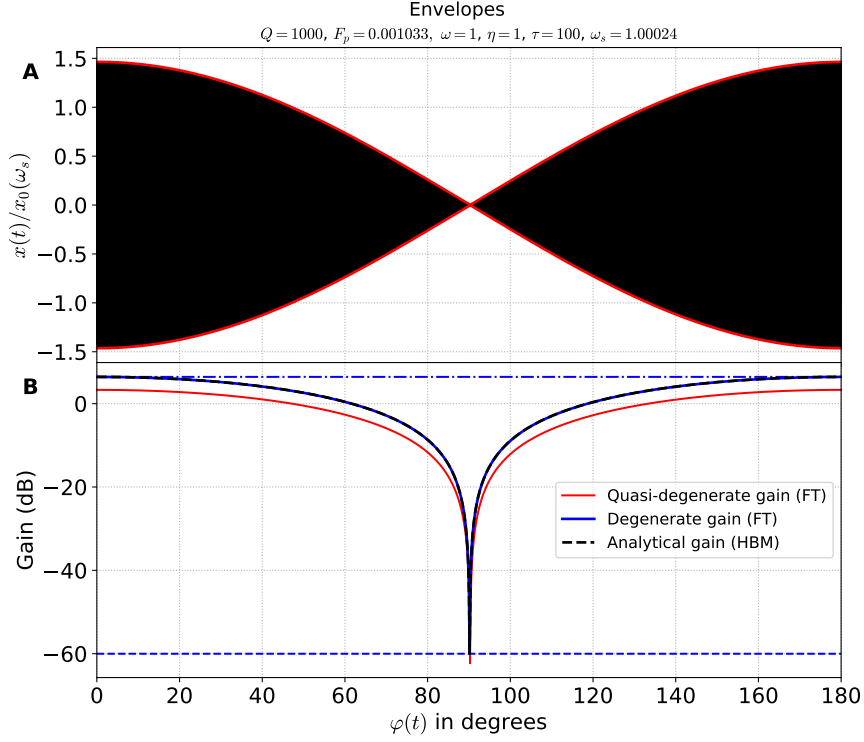


FIG. 4. Gain as a function of phase for the same parametric amplifier with feedback of Fig. 3 with parameters set near the onset of a saddle-node bifurcation. **A** We plot the normalized cyclo-stationary response $x(t)/x_0$ as a function of phase φ , where x_0 is the amplitude of oscillations of the forced harmonic resonator (when $F_p = \eta = 0$). There is a slight detuning between ω and ω_s so that the phase is swept very slowly, almost quasi-statically. The envelopes are obtained from Eq. (23), which are based on FT. **B** We use the positive envelope from **A** to obtain the quasidegenerate gain in decibels. The FT degenerate gain is obtained in Eq. (24). The analytical HBM gain is given in Eq. (15) with the help of Eq. (13). The horizontal lines are the HBM approximations for minimum and maximum gains obtained from Eq. (16).

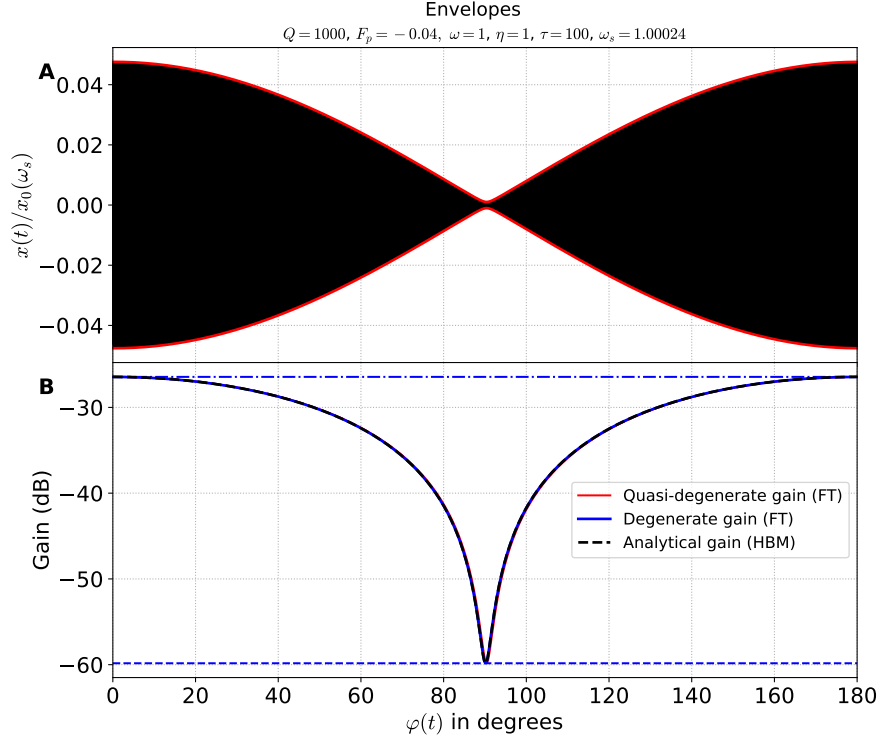


FIG. 5. Gain as a function of phase for the SDOF parametric amplifier with LIA feedback whose dynamics is given in Eq. (3) with parameters set near the onset of a Hopf bifurcation. **A** The response of the SDOF parametric resonator with feedback is far reduced compared with the amplitude of the harmonic oscillator response. **B** There is attenuation in all phases. This indicates that with these parameters the parametric resonator with the proposed feedback scheme leads to cooling.

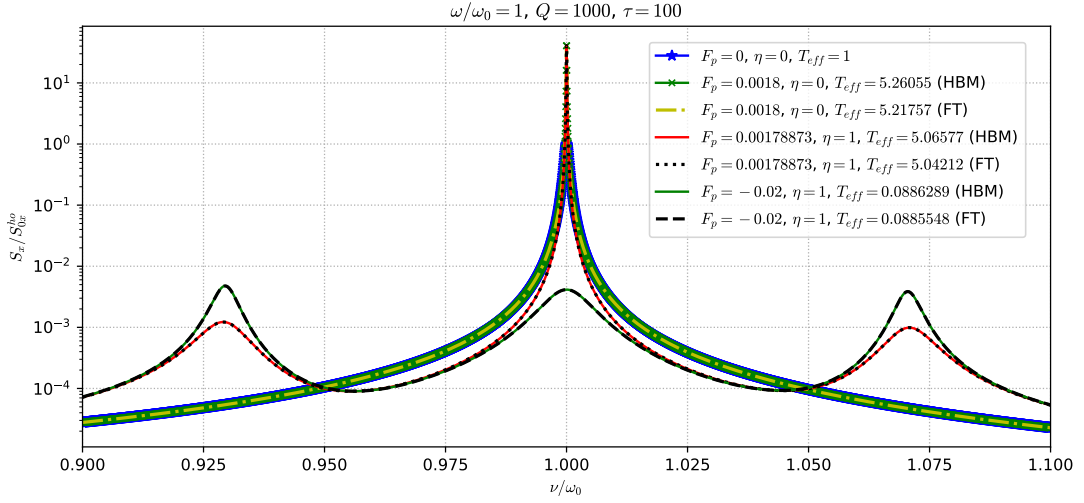


FIG. 6. Noise spectral densities in dB scale: the harmonic oscillator (solid blue line), the SDOF parametric resonator using the harmonic balance method (solid black line) and using FT (dot dashed line), the SDOF parametric resonator with LIA feedback (solid red line, using the HBM, and dotted red line, using FT), with negative pump (solid green line (HBM) and dashed black line (FT)). S_{0x}^{ho} is the peak value of the harmonic oscillator NSD.

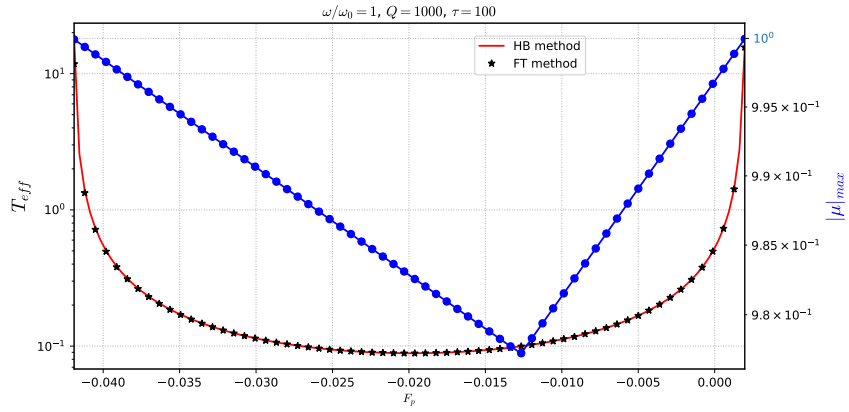


FIG. 7. Effective temperature as a function of pump F_p from the threshold of a Hopf bifurcation (on the left) to the threshold of a saddle-node bifurcation (on the right). Negative F_p indicates there is a π in the pump phase relative to positive pump. The solid line indicates the module of the largest Floquet multiplier whose values can be seen on the right y axis of the figure. The smallest value of this curve corresponds to all Floquet multipliers having the same module.

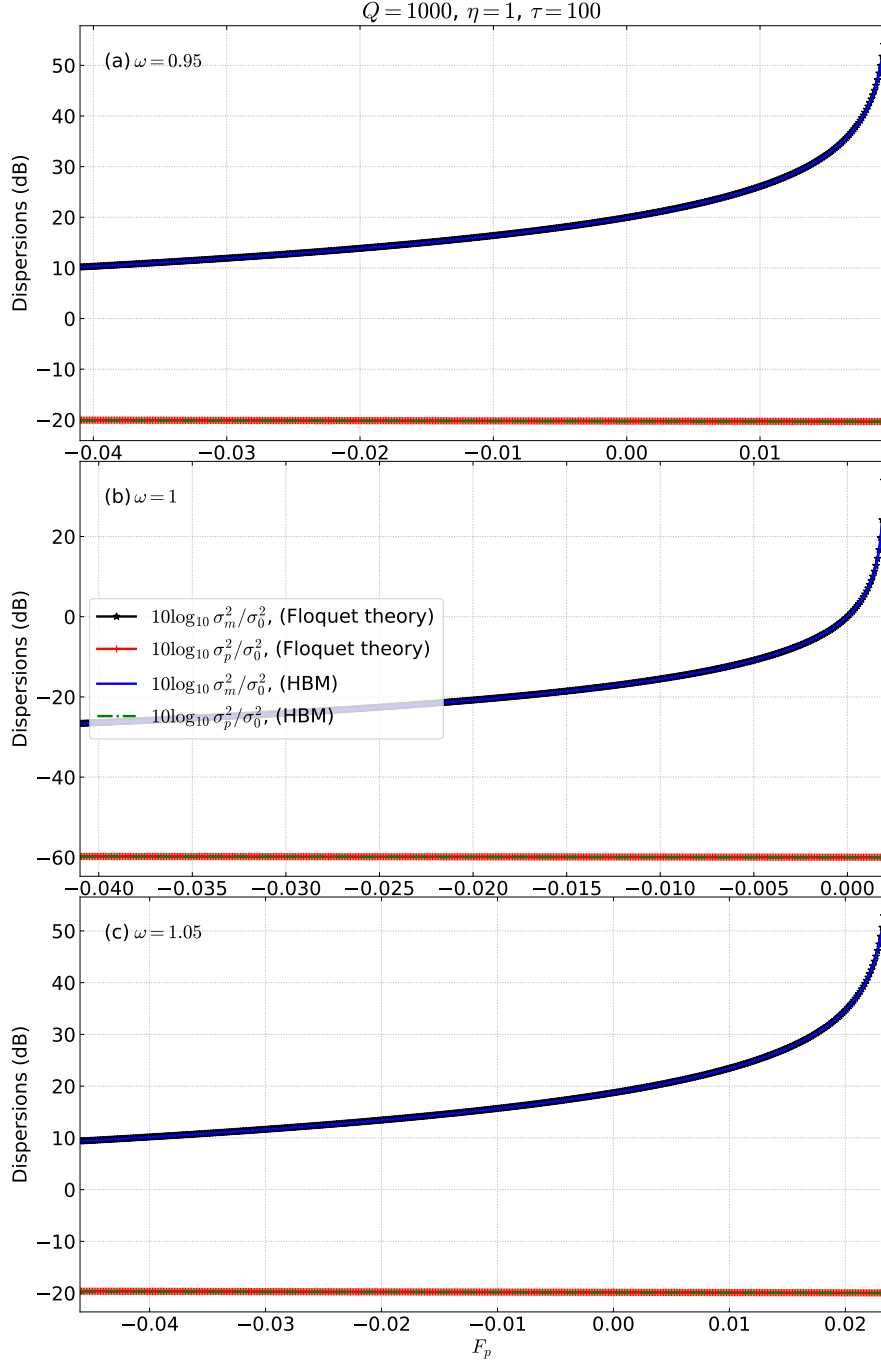


FIG. 8. Floquet theory predictions for the diagonalized standard deviations in decibels relative to the equilibrium values with zero pump in decibel scale in the SDOF parametric resonator with LIA feedback. The results are based on Eqs. (38) where the Green's functions were replaced with the Green's functions with feedback as described in Sec. III B 2. Each plot ends very close to the instability threshold. The common parameters used in all panels are given on top of the figure.

V. CONCLUSION

Here, we have theoretically shown that incorporating feedback into a parametric resonator fundamentally modifies its dynamics. By embedding the feedback into the equations of motion, we were able to apply the same theoretical methods developed in Refs. [28, 29] to analyze its behavior. Due to the feedback scheme, the usual period-doubling bifurcation of SDOF parametric resonators to instability was replaced by a saddle-node bifurcation. Furthermore, the feedback increased the dimension of the dynamical system, what allowed the occurrence of Hopf bifurcations. This opened two distinct ways of controlling fluctuations in the resonator. Our analysis, validated through multiple complementary methods (Fourier analysis, FT, and direct numerical integration of the stochastic differential equations involved) reveals that strong fluctuation suppression can be achieved in two qualitatively different regimes. In one of them, by employing a lock-in amplifier feedback loop, the system's response is no longer limited to the standard parametric squeezing picture (with the -6 dB lower bound [12]). While this is not a new result [14], our analysis sheds more light on it. Near a saddle-node bifurcation, the system exhibits deep squeezing in one of its quadrature fluctuations while it strongly increases the fluctuations in the other quadrature.

The main advance and novelty of this paper is that we analyzed the full impact of the lockin feedback-loop on the response of the parametric resonator to an ac drive or to additive noise. Near a Hopf bifurcation, the feedback induces a regime of strong deamplification and cooling, reducing the oscillator's effective temperature. Simple ringdown experiments could detect the onset of Hopf bifurcations in these systems, while in the frequency domain, the calculation of the noise spectral density provides experimentally accessible signatures of each regime (one main central peak near a saddle-node bifurcation and three peaks with strong sidebands near a Hopf bifurcation). Furthermore, we show that there is an optimal amount of parametric pumping and feedback to reach the strongest cooling. Additionally, we also made estimates on the amount of squeezing that can be achieved in our model.

Although the averaging method may be simpler to apply and has been used extensively in the literature to analyze fluctuations in parametric resonators [1, 14], it fails to capture the onset of Hopf bifurcations, underscoring the necessity of more sophisticated techniques such as Floquet analysis for a complete understanding of the response of such feedback-driven systems to additive noise.

The theoretical framework presented here is general and could be applied to a wide range

of physical implementations, from nano-mechanical resonators and superconducting circuits to trapped ions and cold atoms. The two bifurcations identified provide a clear experimental target: parameters can be chosen to either cool the system towards its quantum ground state or to generate squeezed states necessary for back-action-evading measurements [32]. Furthermore, extending this analysis to the quantum regime presents an stimulating, yet challenging, direction for future research. For instance, the methods developed here could be applied to reduce phase-flip errors in phase states of Josephson (or Kerr) parametric oscillators in the presence of noise, an essential step for the realization of qubit quantum gates in these systems [10, 33].

VI. APPENDIX: THE LOCKIN AMPLIFIER OPERATION

The two-phase LIA is essential for observing and measuring thermo-mechanical squeezing [12]. Therefore, we discuss briefly about its key features that we believe could be helpful for readers, especially those who are not familiar with its applications and internal mechanisms. In Fig. 9, we can see a simple block diagram of a lockin amplifier, adapted from a Zurich Instruments white paper [34]. The LIA allows the detection of very small signals buried inside noise. This is possible because the multiplication stage of the LIA is performed before the detected analog signal is digitalized. In the conversion from analog to digital signals, the vertical resolution of the LIA is limited by the input voltage range and by the number of bits used in the discretization of the input analog values. In the simplest configuration the input signal of the LIA is the response $x(t)$ of the parametric resonator to additive noise. This input signal is split into the two LIA channels in quadrature: a cosine and a sine channel. In the cosine channel the input signal is multiplied by a cosine wave at half the pump frequency and fed to a low-pass filter (LPF), while in the sine channel this signal is multiplied by a sine wave at half the pump frequency and fed to a second LPF. In the model studied here, each of the lockin LPFs consists of only one low-pass RC filter with a time constant $\tau = RC$. The lockin outputs $X_L(t)$ and $Y_L(t)$ are known as the cosine and sine quadratures, respectively. The mathematical expressions for $X_L(t)$ and $Y_L(t)$ are given by

$$\begin{aligned} X_L(t) &= \frac{1}{\tau} \int_{-\infty}^t e^{-(t-t')/\tau} \cos(\omega t') x(t') dt', \\ Y_L(t) &= \frac{1}{\tau} \int_{-\infty}^t e^{-(t-t')/\tau} \sin(\omega t') x(t') dt'. \end{aligned} \tag{A.1}$$

It is important to calculate the Fourier transforms of $X_L(t)$ and $Y_L(t)$ given in Eq. (A.1). We

find

$$\begin{aligned}\tilde{X}_L(\nu) &= \int_{-\infty}^{\infty} e^{i\nu t} X_L(t) dt = \frac{1}{\tau} \int_{-\infty}^{\infty} e^{t'/\tau} \cos(\omega t') dt' \int_{t'}^{\infty} e^{-(1/\tau - i\nu)t} dt = \frac{\tilde{x}(\nu + \omega) + \tilde{x}(\nu - \omega)}{2(1 - i\nu\tau)}, \\ \tilde{Y}_L(\nu) &= \int_{-\infty}^{\infty} e^{i\nu t} Y_L(t) dt = \frac{1}{\tau} \int_{-\infty}^{\infty} e^{t'/\tau} \sin(\omega t') dt' \int_{t'}^{\infty} e^{-(1/\tau - i\nu)t} dt = \frac{\tilde{x}(\nu + \omega) - \tilde{x}(\nu - \omega)}{2i(1 - i\nu\tau)}.\end{aligned}\quad (\text{A.2})$$

Hence, we obtain $\tilde{X}_L(0) = \tilde{x}'(\omega)$ and $\tilde{Y}_L(0) = \tilde{x}''(\omega)$. This result is independent of the LIA time constant τ .

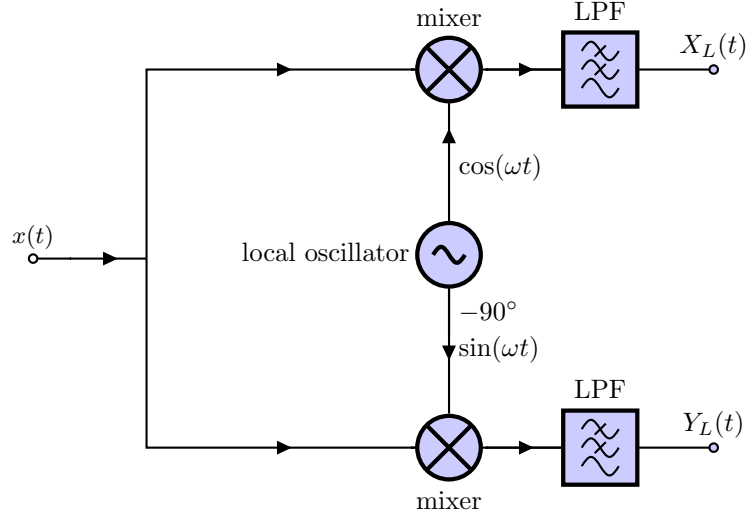


FIG. 9. The two-phase lockin amplifier block diagram. The low pass filters are RC filters with the same time constant. The mixers are multipliers.

-
- [1] A. Bachtold, J. Moser, and M. Dykman, *Rev. of Mod. Phys.* **94**, 045005 (2022).
 - [2] J. Aasi *et al.*, *Nature Photonics* **7**, 613–619 (2013).
 - [3] S. E. Dwyer, G. L. Mansell, and L. McCuller, *Galaxies* **10**, 46 (2022).
 - [4] M. Aspelmeyer, T. J. Kippenberg, and F. Marquardt, *Rev. of Mod. Phys.* **86**, 1391 (2014).
 - [5] X. You, Z. Li, and Y. Li, *Phys. Rev. A* **96**, 063811 (2017).
 - [6] C. Zhao, X. Zhou, M. Pandit, G. Sobreviela, S. Du, X. Zou, and A. Seshia, *Physical Review Applied* **12**, 044005 (2019).
 - [7] J. Moser, J. Güttinger, A. Eichler, M. J. Esplandiu, D. Liu, M. Dykman, and A. Bachtold, *Nature Nanotechnology* **8**, 493 (2013).

- [8] W. Zhang and K. L. Turner, *Sensors and Actuators A: Physical* **122**, 23 (2005).
- [9] L. Papariello, O. Zilberberg, A. Eichler, and R. Chitra, *Phys. Rev. E* **94**, 022201 (2016).
- [10] A. Grimm, N. E. Frattini, S. Puri, S. O. Mundhada, S. Touzard, M. Mirrahimi, S. M. Girvin, S. Shankar, and M. H. Devoret, *Nature* **584**, 205 (2020).
- [11] H. Shen and N. Yoshikawa, *Superconductor Science and Technology* **39**, 015001 (2026).
- [12] D. Rugar and P. Grütter, *Phys. Rev. Lett.* **67**, 699 (1991).
- [13] A. N. Cleland, *New Journal of Physics* **7**, 235 (2005).
- [14] A. Vinante and P. Falferi, *Phys. Rev. Lett.* **111**, 207203 (2013).
- [15] M. Poot, K. Y. Fong, and H. Tang, *New Journal of Physics* **17**, 043056 (2015).
- [16] S. Sonar, V. Fedoseev, M. J. Weaver, F. Luna, E. Vlieg, H. van der Meer, D. Bouwmeester, and W. Löffler, *Phys. Rev. A* **98**, 013804 (2018).
- [17] A. Mashaal, L. Stefan, A. Ranfagni, L. Catalini, I. Chernobrovkin, T. Capelle, E. C. Langman, and A. Schliesser, *Physical Review Research* **7**, L012071 (2025).
- [18] T. Briant, P. Cohadon, M. Pinard, and A. Heidmann, *The European Physical Journal D* **22**, 131–140 (2003).
- [19] J. Gieseler, B. Deutsch, R. Quidant, and L. Novotny, *Phys. Rev. Lett.* **109**, 103603 (2012).
- [20] J. Gao, F. van der Laan, J. A. Zielińska, A. Militaru, L. Novotny, and M. Frimmer, *Physical Review Research* **6**, 033009 (2024).
- [21] A. Hopkins, K. Jacobs, S. Habib, and K. Schwab, *Phys. Rev. B* **68**, 235328 (2003).
- [22] M. Poggio, C. Degen, H. Mamin, and D. Rugar, *Phys. Rev. Lett.* **99**, 017201 (2007).
- [23] J. Guo, R. Norte, and S. Gröblacher, *Phys. Rev. Lett.* **123**, 223602 (2019).
- [24] U. Delić, M. Reisenbauer, K. Dare, D. Grass, V. Vuletić, N. Kiesel, and M. Aspelmeyer, *Science* **367**, 892–895 (2020).
- [25] A. Schliesser, O. Arcizet, R. Rivière, G. Anetsberger, and T. J. Kippenberg, *Nature Physics* **5**, 509–514 (2009).
- [26] O. Arcizet, P.-F. Cohadon, T. Briant, M. Pinard, and A. Heidmann, *Nature* **444**, 71–74 (2006).
- [27] A. D. O’Connell, M. Hofheinz, M. Ansmann, R. C. Bialczak, M. Lenander, E. Lucero, M. Neeley, D. Sank, H. Wang, M. Weides, J. Wenner, J. M. Martinis, and A. N. Cleland, *Nature* **464**, 697 (2010).
- [28] A. A. Batista, *Physica Scripta* **99**, 065258 (2024).
- [29] A. A. Batista, R. S. Moreira, and A. L. de Souza, *Physica A* **671**, 130603 (2025).
- [30] A. A. Batista, [arXiv:2501.06991](https://arxiv.org/abs/2501.06991) (2025), 10.48550/arXiv.2501.06991.

- [31] A. A. Batista, A. A. L. de Souza, and R. S. N. Moreira, *J. of Appl. Phys.* **132**, 174902 (2022).
- [32] R. Schnabel, *Physics Reports* **684**, 1 (2017).
- [33] G. Lakshmi Bhai, H. Mukai, T. Yamamoto, and J.-S. Tsai, *Physical Review Applied* **19**, 014065 (2023).
- [34] Zurich Instruments, Whitepaper: “Principles of lock-in detection and the state of the art” (2016).